Archival Report

Biological Psychiatry

Four Distinct Subtypes of Alzheimer's Disease Based on Resting-State Connectivity Biomarkers

Pindong Chen, Hongxiang Yao, Betty M. Tijms, Pan Wang, Dawei Wang, Chengyuan Song, Hongwei Yang, Zengqiang Zhang, Kun Zhao, Yida Qu, Xiaopeng Kang, Kai Du, Lingzhong Fan, Tong Han, Chunshui Yu, Xi Zhang, Tianzi Jiang, Yuying Zhou, Jie Lu, Ying Han, Bing Liu, Bo Zhou, and Yong Liu, for the Alzheimer's Disease Neuroimaging Initiative

ABSTRACT

BACKGROUND: Alzheimer's disease (AD) is a neurodegenerative disorder with significant heterogeneity. Different AD phenotypes may be associated with specific brain network changes. Uncovering disease heterogeneity by using functional networks could provide insights into precise diagnoses.

METHODS: We investigated the subtypes of AD using nonnegative matrix factorization clustering on the previously identified 216 resting-state functional connectivities that differed between AD and normal control subjects. We conducted the analysis using a discovery dataset (n = 809) and a validated dataset (n = 291). Next, we grouped individuals with mild cognitive impairment according to the model obtained in the AD groups. Finally, the clinical measures and brain structural characteristics were compared among the subtypes to assess their relationship with differences in the functional network.

RESULTS: Individuals with AD were clustered into 4 subtypes reproducibly, which included those with 1) diffuse and mild functional connectivity disruption (subtype 1), 2) predominantly decreased connectivity in the default mode network accompanied by an increase in the prefrontal circuit (subtype 2), 3) predominantly decreased connectivity in the anterior cingulate cortex accompanied by an increase in prefrontal cortex connectivity (subtype 3), and 4) predominantly decreased connectivity in the basal ganglia accompanied by an increase in prefrontal cortex connectivity (subtype 4). In addition to these differences in functional connectivity, differences between the AD subtypes were found in cognition, structural measures, and cognitive decline patterns.

CONCLUSIONS: These comprehensive results offer new insights that may advance precision medicine for AD and facilitate strategies for future clinical trials.

https://doi.org/10.1016/j.biopsych.2022.06.019

Alzheimer's disease (AD) is a neurodegenerative disorder that shows phenotypic heterogeneity in its clinical profile, imaging features, pathology, and disease progression (1). Typical clinical representation of AD is an initial amnestic-predominant impairment with a predominant early distribution of neurofibrillary tangle pathology in the medial temporal lobe; atypical AD subtypes show differences in spatial patterns of tau pathology and cognitive decline profiles (2–4). Atypical phenotypes might lead to more misdiagnosis and delayed diagnosis for atypical AD when assessed using the current biomarker-based diagnostic criteria (3,5,6). Moreover, distinct pathological patterns may affect treatment responses (7,8), and different subtypes may have distinct trajectories of cognitive decline (9,10), potentially affecting clinical trials. For these reasons, research on the heterogeneity of AD is needed to reveal ways to control the various phenotypes and further contribute to personalized medicine (1).

The heterogeneity of AD has been investigated based on neurobiological characteristics in autopsies and in vivo (4). Individuals with AD who showed differences in the primary location of the neurofibrillary tangles were divided into 3 subtypes, i.e., limbic-predominant, hippocampal-sparing, and typical, in several large-scale postmortem studies (11–13). Atypical subtypes of AD with different impairment patterns and cognitive profiles have also been investigated based on in vivo patterns found through structural magnetic resonance imaging (MRI) (9,14–21), diffusion tensor imaging (22), and fluorodeoxyglucose positron emission tomography (FDG-PET) (23). Atypical spread patterns of neuropathology were also found by using tau-PET (24–26) and amyloid-PET (27). However, the heterogeneity of functional networks that is closely related to cognition has not been well studied (4).

Widespread disruptions in resting-state functional networks are observed in AD, suggesting that there is not only local functional activity damage in the neuron loss area but also global network impairment (28–33). More importantly, variability in tau patterns coincides with functional networks, and the spread of tau and amyloid-β burden is associated

SEE COMMENTARY ON PAGE 752

ISSN: 0006-3223

with the altered functional connectivity (34–37), suggesting that functional brain networks are involved in the heterogeneous neurobiology of AD (38). Different alterations in functional network properties were reported in AD atrophy subtypes (39), but the results were restricted to the anatomical subtypes and could not provide a comprehensive understanding of the heterogeneous functional network in AD. We previously used a large multicenter dataset to show 216 functional connectivities that differed between patients with AD and normal control subjects (NCs), and our results revealed that these connectivities could be used to accurately discriminate patients with AD with high generalizability (40). These functional signatures also showed a clustered pattern, inspiring us to continue to investigate whether different functional subtypes are associated with specific network patterns in AD.

In this study, we directly investigated the hypothesis that functional networks are heterogeneously altered in AD and that this heterogeneity can explain the variations in cognitive impairments and structural alterations. To test these hypotheses, we applied nonnegative matrix factorization (NMF) clustering to identify the functional subtypes of AD and mild cognitive impairment (MCI) using 2 multicentric datasets with large samples and further investigated the differences in functional connectivity, brain structure, and clinical cognitive ability between the subtypes (Figure 1).

METHODS AND MATERIALS

Subjects

We first identified subtypes of patients with AD from the Multi-Center Alzheimer Disease Imaging Consortium (MCADI) dataset, which served as a discovery dataset (AD: n = 295, MCI: n = 257, NC: n = 257). A total of 291 subjects (AD: n = 82, MCI: n = 93, NC: n = 116) from the Alzheimer's Disease Neuroimaging Initiative (ADNI) (http://adni.loni.usc.edu) dataset were included as an independent validation set. For detailed information, see Supplemental Method S1.

Definition of Image Acquisition, Preprocessing, and Clustering Features

In the discovery dataset, individuals were scanned on 1 of 7 different MRI scanners to obtain T1-weighted images and resting-state functional images (41). In the ADNI dataset, T1-weighted images and resting-state functional images were scanned using standardized protocols at each site (http://adni.loni.usc.edu/methods/mri-tool/mri-acquisition/).

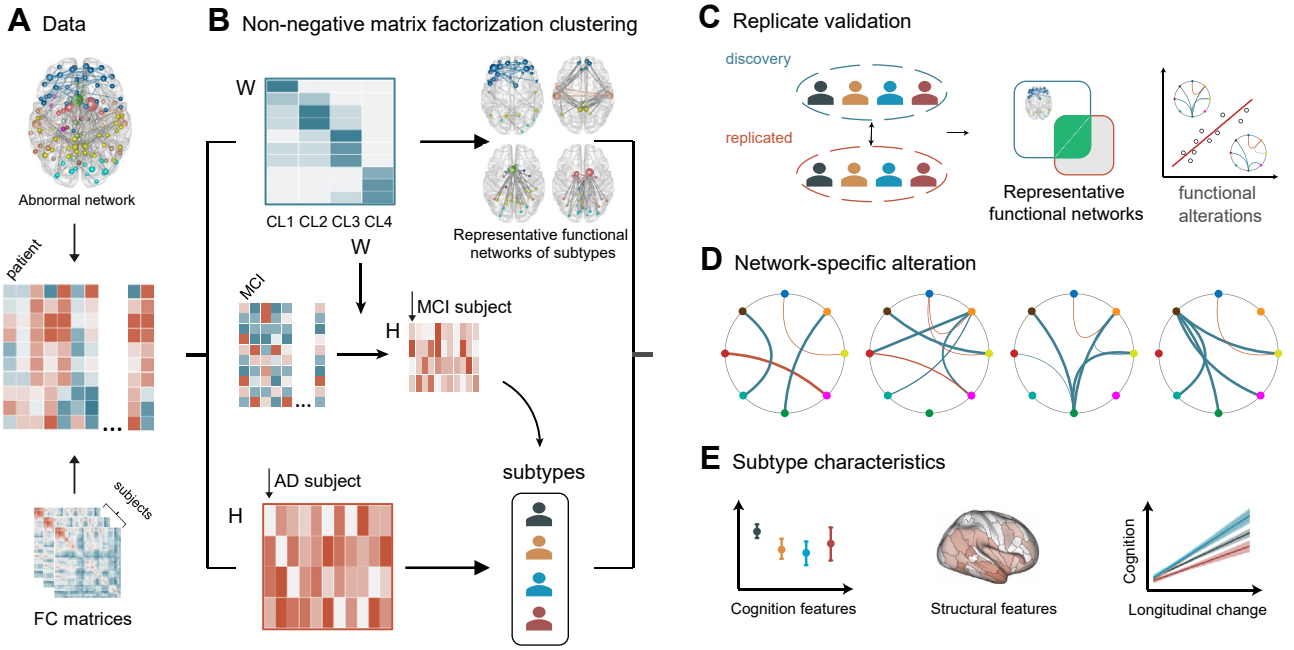

Figure 1. Schematic of the heterogeneity analysis pipeline. **(A)** The data used were based on a functional connectivity (FC) matrix constructed from the Brainnetome Atlas and an abnormal functional connectivity index from a previous study (40). **(B)** In patients with Alzheimer's disease (AD), the nonnegative matrix factorization was applied to simultaneously identify clusters of features and subjects. (Top) Each row represents a functional connection and each column is a functional connectivity cluster. The more saturated the color, the greater the contribution of functional connectivity to the functional connectivity cluster. The functional connectivities within the abnormal functional network were clustered into 4 functional connectivity clusters, which could be represented by representative functional network (RFNs). (Bottom) Each column represents 1 subject and the more saturated the color, the greater the contribution of that RFNs to the subject's abnormal functional network. Subjects with AD were clustered into different subtypes based on the minimum contribution of RFNs. (Middle) The individuals with mild cognitive impairment (MCI) were assigned based on the clustering identified for AD. **(C)** Replication analysis was applied on an independent dataset to validate the reproducibility of the subtypes, which compared the RFNs of the subtypes and the alterations associated with the subtypes between the 2 datasets. **(D)** The network-specific alterations of the subtypes were investigated by comparing the patients with AD subtypes to the normal control subjects. **(E)** Statistical analyses, including clinical measures comparisons, regional structural features comparisons, and cognition decline trajectories, were applied to uncover the characteristics of the subtypes. CL, cluster.

The corresponding MRI acquisition protocols are described in Supplemental Method S2 and Table S2, as well as in our previous studies (40–42).

The structural MRI images were preprocessed using the standard steps in the CAT12 toolbox (r1450) (http://dbm.neuro.uni-jena.de/cat/) and the regional gray matter volume and cortical thickness of each brain region were extracted according to the Brainnetome Atlas (43). ComBat harmonization (https://github.com/rpomponio/neuroHarmonize) was applied to pool the data from MCADI and ADNI by removing the site effects (44,45), with age, sex, and clinical diagnosis as covariates.

Functional MRI (fMRI) scans from the MCADI and ADNI were preprocessed using the Brainnetome Toolkit (http://brant.brainnetome.org) (46). After quality control, we derived a regional fMRI signal for each of the 263 regions by averaging the fMRI signal across all the voxels included in the region. The detailed information is described in our previous study (40) and Supplemental Method S3B.

Functional connectivity for each individual was measured using Pearson's correlation coefficients between all pairs of 263 regions. Then, 216 abnormal functional connectivities, which were derived from a meta-analysis of the first 6 data sites in the MCADI that was performed in our previous study, were used directly as clustering features and were designated the abnormal functional network (AFN) (40) (Supplemental Method S4 and Table S3). Next, ComBat harmonization was applied to the clustering features to reduce site effects, with age, sex, and clinical diagnosis as covariates in the MCADI and ADNI (44,45,47).

Cluster Analysis Using NMF

To investigate AD subtypes, we used NMF to perform a cluster analysis based on the functional connectivities that are in the AFN in the patient group (Figure 1B) (48). As a data-driven dual-clustering approach, NMF allows the simultaneous identification of clusters of features (e.g., functional connectivity) and clusters of individuals according to the weights of feature clusters in the database, which means we can obtain the functional connectivity clusters and the weight of each functional connectivity cluster for each individual. We characterized each feature cluster based on the top 20% weighted functional connectivities of each cluster, which were designated the representative functional network (RFN) to represent the functional connectivity cluster. Because AD is associated with functional dysfunction and disconnection mechanisms (28), subjects were grouped into subtypes based on the minimum weight (highest disconnection) of RFNs to the subjects' functional connectivity within the AFN. To obtain the corresponding subtypes in MCI, we used the fitted NMF model for AD to factorize the functional connectivity data of MCI (Supplemental Method S5A).

We determined the optimal number of clusters by assessing the cophenetic correlation coefficient, the silhouette coefficient, and the changes in the residual sum of squares (Supplemental Method S5B) (20,49). We implemented the NMF algorithm based on the NMF package (http://renozao.github.io/NMF) (50) in R (version 3.6.3).

Statistical Analysis

Appropriate analysis of variance and/or a two-sample t test were applied to identify the difference in the functional connections (after Fisher's z transformation), cognition, and structural features between each AD subtype and NCs ($p < .05$). We compared functional connections between subtypes for each dataset separately, and other clinical features were z-transformed and pooled across datasets. Next, we analyzed the longitudinal changes in the cognitive measures between the AD subtypes using the 3-year follow-up data in the ADNI dataset (Table S4). A linear regression model was used to assess the differences in the longitudinal changes between subtypes. The number of months of follow-up from baseline, subtype, age, sex, and the interaction term for the months and subtypes were included in the model ($p < .05$). Finally, the gray matter volumes and cortical thickness of the regions in Brainnetome Atlas were compared between the subtypes to elucidate the relationship between functional subtypes and structural subtypes (4,51,52). The above comparisons were performed after controlling for sex, age, site, and total intracranial volume (only in structural features) (53). Detailed information can be found in Supplemental Method S7.

Data Availability

The data that support the findings of this study are available from the corresponding author upon reasonable request. All ADNI data are deposited in a publicly accessible repository and can be accessed at the ADNI website (http://adni.loni.usc.edu/). The code that was used can be obtained at GitHub (https://github.com/YongLiuLab).

RESULTS

Four Subtypes Identified in AD

In total, 4 clusters showed an optimal fit according to the cophenetic coefficient, silhouette coefficient, and the residual sum of squares changes in the MCADI and ADNI (Supplemental Results S1 and Figure S2).

Figure 2A shows the RFN (i.e., the functional connectivity that contributed to the top 20% of the functional connectivity cluster) of each subtype representing each subtype's specific network in the 2 datasets (also see Figure S3). It is worth noting that the 2 results showed similar patterns and that the Dice coefficients between the 4 RFNs of the MCADI and those of the ADNI were 0.72, 0.76, 0.72, and 0.88, respectively (Figure 2B). To precisely describe the specific network, the composite RFN of each subtype was obtained by extracting the intersections of the 2 results (Figure 2C). Subtype 1 was specifically associated with the prefrontal lobe and a widespread frontal-parietal-occipital network. Subtype 2 was associated explicitly with functional connections in the medial prefrontal lobe, medial temporal lobe, hippocampus, and parietal lobe; these areas are similar to the areas of the default mode network (DMN). Subtype 3 was characterized by functional connections that connected the anterior cingulate cortex to other regions, especially the parietal lobe, basal ganglia, and occipital lobe. The top functional connections of the RFN of subtype 4 connected the basal ganglia (mainly in the bilateral dorsal caudate) with the cerebellum, occipital lobe, temporal

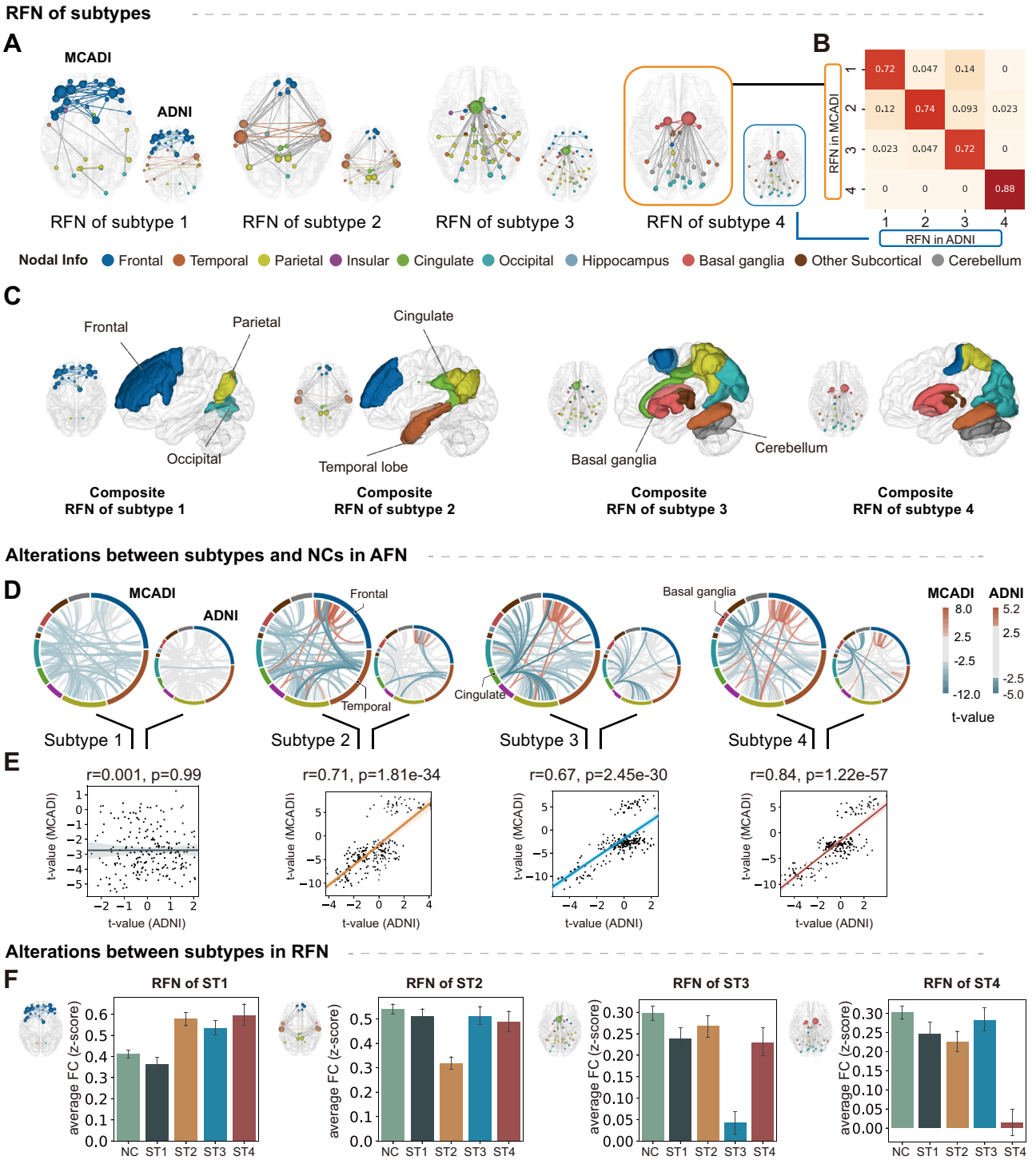

Figure 2. Functional subtyping results for Alzheimer's disease (AD). **(A)** Illustration of the representative functional networks (RFNs) of 4 subtypes. The larger brain represents the results from the Multi-Center Alzheimer Disease Imaging Consortium (MCADI) dataset, while the smaller brain to the right represents the results from the Alzheimer's Disease Neuroimaging Initiative (ADNI). The size of the node in the brain represents the relative number of abnormal connections linked to the node. **(B)** Reproducibility between the 2 datasets. The heatmap shows the Dice coefficients for the spatial similarity between the 4 RFNs in the 2 datasets. **(C)** Illustration of the composite RFNs. Composite RFNs were derived from the intersection of the results from the 2 datasets. **(D)** Alterations within the abnormal functional network (AFN) for the 4 subtypes compared with the normal control subjects (NCs), in which the larger circle represents the results from the MCADI while the smaller brain to the right represents the results from the ADNI. The band color in the circular figure corresponds to the color of the brain node, and the connection color represents the *t* value derived from a *t* test between the patients with AD and the NCs. **(E)** Scatter plot showing the

lobe, and thalamus. Subtypes were reproducible among the different brain atlases and control of head motion, with and without ComBat (Figures S4–S6 and Supplemental Results S2–S4) (54).

Functional Characterization of Subtypes in AD

In comparison with NCs, individual clustering results showed that patients with different subtypes had complex impairments in functional connectivity, which were associated with multiple RFNs. Subtype 1 showed mild and diffuse reduced alterations in the AFN compared with the NCs, while the other subtypes showed increased alterations in the prefrontal lobe (mainly in the RFN of subtype 1) and different, predominantly reduced connections that were specific to the various corresponding RFNs (Figure 2D). Similar altered functional connectivity patterns were found in the ADNI data. The alterations of whole-brain functional connectivity are shown in Figure S8. In addition, the altered strength (t value) of the connectivity in patients with AD in comparison with that of the NCs showed significant correlations between the MCADI and ADNI datasets (Pearson's correlation coefficients r = 0.71, 0.67, and 0.84, respectively) for subtypes 2, 3, and 4 (Figure 2E), a finding that indicated that the results are reproducible. Because the clusters showed similar features across the 2 datasets, we pooled the participants of each subtype across the datasets for further analysis.

Figure 2F shows the specific alterations in the average functional connectivity of RFNs in the subtypes. The results showed that network-specific alterations could be identified in the subtypes, as mentioned previously (Figure 2D), and that subtype-specific alterations are present in the RFNs. In brief, the average functional connectivity of the RFN associated with each corresponding subtype was significantly weaker than that associated with the other subtypes (Table S5).

Demographic and Cognitive Characterization of Subtypes

Figure 3A shows the ratio of subtypes for each data site; each site included the 4 subtypes, and each subtype included both male and female patients with AD. The distribution of the subtypes among the 7 sites in the MCADI showed that 90 patients were grouped into subtype 1, 94 patients were grouped into subtype 2, 70 patients were grouped into subtype 3, and 41 patients were grouped into subtype 4. The numbers of samples allocated to the 4 clusters were 27, 26, 14, and 15, respectively, in the ADNI.

Figure 3B shows functionally defined subtypes of AD showing demographic and cognitive differences. Age differed between subtypes (F_{294} = 4.45, p = .004), with the participants with subtype 3 being older than those of subtype 1 ($p < .001$), subtype 2 (p = .007), or subtype 4 (p = .25). All subtypes showed similar proportions of females (p = .24). Patients with subtype 1 had higher Mini-Mental State Examination (MMSE) scores (F_{294} = 4.71, p = .003) than those in subtype 2 (p = .001), subtype 3 ($p < .001$), or subtype 4 (p = .026). Moreover, the MMSE and the average functional connectivity of RFNs of subtypes had a significant Pearson correlation ($r = -0.16$, p = .006) in RFN1 after controlling for age, sex, and site (Figure S9). Subtype 2 and subtype 4 showed worse performance on word learning ability in the Auditory Verbal Learning Test (F_{179} = 5.55, p = .002) than subtype 1 ($p < .001$ and p = .007, respectively) and subtype 3 (p = .011 and p = .055, respectively) (Table S6). Apart from overall cognitive ability, there was no significant finding from the analysis of variance models of the composite cognitive scores in the ADNI dataset. Subtype 1 showed the best executive, memory, and visuospatial (ADNI-composite measures for visuospatial functioning [ADNI-VS]) function numerically, whereas subtype 4 showed the worst ADNI-VS function numerically (Figure 3C). The 4 AD subtypes showed differences in the cognitive decline progression. Although subtype 1 had the better cognitive ability at baseline, there was only a slow ADNI-VS decline and the other cognitive decline trajectories were similar to those of subtype 4. Subtype 2 showed the fastest decline in the MMSE and ADNI-VS, and subtype 3 had the slowest decline in the MMSE (Figure 3D; Tables S7–S10).

Moreover, MCI was clustered based on the AD subtype patterns (Figure 3A). MCI subtypes showed similar characteristics to those found for AD, and the corresponding information can be found in Supplemental Results S5 and Figure S10.

Structural Characterization of Subtypes of AD

The gray matter volumes of the frontal lobe, temporal lobe, parietal lobe, occipital lobe, and cingulate cortex differed between the subtypes (all ps $<.05$, Bonferroni corrected), but the volumes of the occipital lobe, hippocampus, and basal ganglia showed no significant difference after Bonferroni correction. Figure 4A shows the mean gray volume, indicating that subtype 1 had the highest volume of the 4 subtypes, but the other 3 subtypes showed only small differences (Table S11 for details about all the above results).

Figure 4B shows the one-to-other cortical thickness comparisons, and Figure 4C shows the uncorrected paired comparisons to demonstrate the small differences between subtypes. Compared with other subtypes, subtype 1 had the greatest cortical thickness in most of the areas, including in the frontal lobe, temporal lobe, and cingulate gyrus, as well as had more gray matter volume in subcortical areas, including the thalamus, hippocampus, and basal ganglia ($p < .05$, false discovery rate [FDR] corrected) (Figure S13). Subtype 2 had the smallest cortical thickness mainly in the precuneus, fusiform gyrus, orbital gyrus, and left middle temporal gyrus ($p < .05$, FDR corrected). Subtype 3 had large cortical thickness in the paracentral lobule and precuneus and a smaller volume in the anterior and ventral cingulate cortex ($p < .05$, FDR corrected). Subtype 4 had relatively lower cortical thickness mainly in the right cingulate cortex, right middle temporal gyrus, right orbital gyrus, and right occipital cortex ($p < .05$, FDR corrected).

relationship between the unthresholded t values derived from comparisons between the patients with AD and the NCs within the abnormal network in the 2 datasets separately, and a higher correlation indicates more similar alteration patterns in AD between the 2 datasets. **(F)** Average functional connectivity of 4 composite RFNs of the 4 AD subtypes with that of the NCs as a reference (the error bar represents the standard errors). ST, subtype.

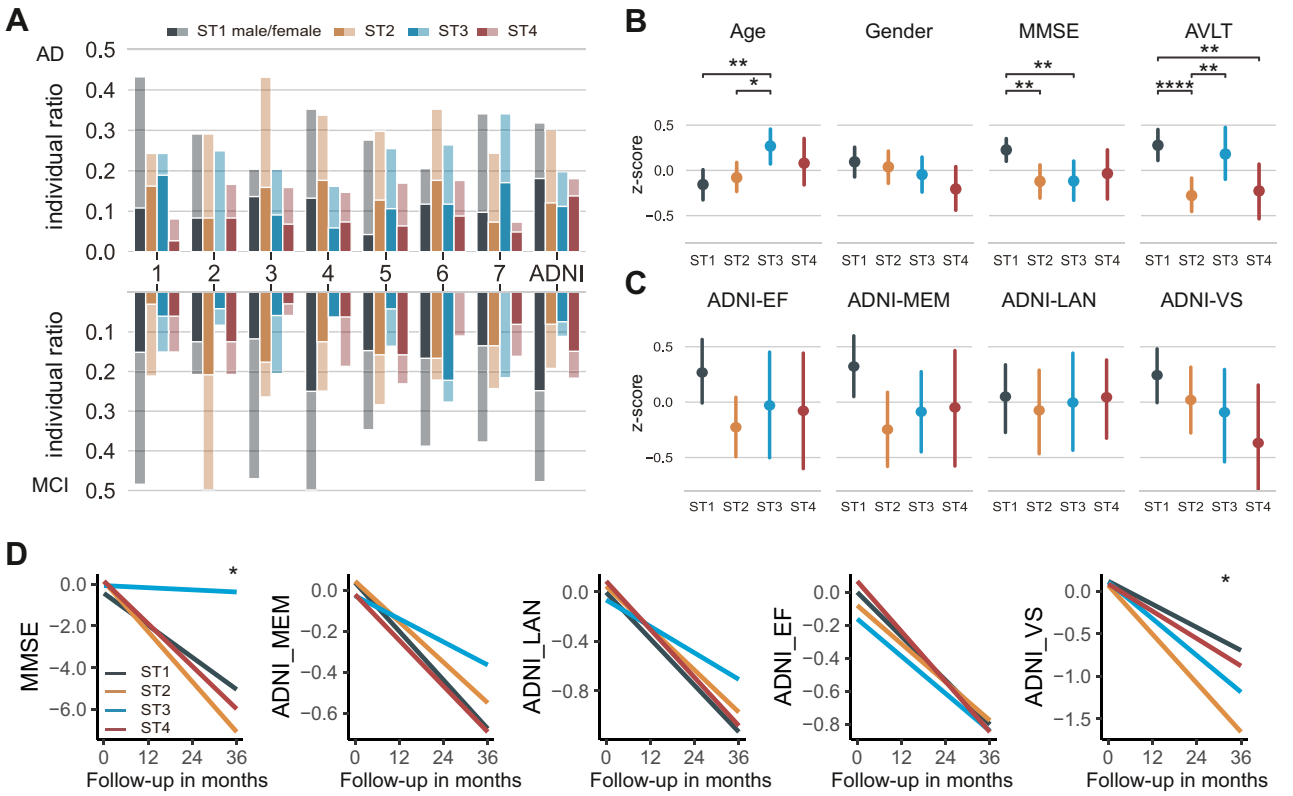

Figure 3. Characteristics of the Alzheimer's disease (AD) subtypes. **(A)** Distribution of the AD and mild cognitive impairment (MCI) subtypes in the 7 data sites of the Multi-Center Alzheimer Disease Imaging Consortium (MCADI) and the Alzheimer's Disease Neuroimaging Initiative (ADNI). **(B)** Comparisons of common demographic and cognitive characteristics between the subtypes in the 2 datasets. **(C)** Comparisons of the composite scores between the subtypes in the ADNI dataset. **(D)** Longitudinal changes in the cognitive ability in the ADNI dataset. The graphs illustrate regression lines from the baseline to a 36-month follow-up, and the * represents significant differences in the decline ratios between subtypes. Data are presented as *z* scores in **(B)** and **(C)**; $^{*}p < .05$, $^{**}p < .01$, $^{****}p < .0001$. AVLT, Auditory Verbal Learning Test; EF, executive function; LAN, language; MEM, memory; MMSE, Mini-Mental State Examination; ST, subtype; VS, visuospatial function.

DISCUSSION

To our knowledge, this is the first effort to identify precise functional network–specific subtypes using large resting-state fMRI biobanks of patients with AD. Our results provided consistent evidence in that the 4 AD subtypes were derived from abnormal functional connectivity data from 2 independent datasets. More importantly, these 4 subtypes had differences not only in functional phenotypes but also in cognitive ability and spatial atrophy patterns. These findings provide supportive evidence for the heterogeneity of functional connectivity in AD.

There is a consensus that the neurobiology of AD is heterogeneous (52,55,56), and convergent evidence based on the availability of large-scale brain structure, pathophysiological, neuropathological, cognitive, or biological datasets have supported disease heterogeneity (4,52,55,57,58). Owing to the absence of extensive multicentric studies, derived functional network alteration was still not well investigated until a previous multicenter reproducibility study was conducted (40). Based on a mega-analysis, Jin *et al.* (40) provided a comprehensive picture of widespread dysconnectivity in AD by clustering the altered functional connectivities in the AFN. Here, we further extended that work by studying disease heterogeneity within AD. Our findings revealed at least 4 distinct, reproducibly altered patterns in functional connectivity in AD, including one with diffuse and mild functional connectivity disruption (subtype 1), one in which decreased functional connectivity of the DMN predominated with an increase in prefrontal connectivity (subtype 2), one in which a decreased functional connectivity of the ACC predominated with an increase in prefrontal connectivity (subtype 3), and one in which a decreased functional connectivity of the basal ganglia predominated with an increase in prefrontal connectivity (subtype 4). Because the mean strength of the RFN, the brain atrophy patterns, and the trend of the longitudinal cognition changes are particularly subtype specific, our findings indicate that the different functional subtypes might be associated with different therapeutic monitoring frameworks.

The science of brain networks provides novel insights into how the brain works and becomes dysfunctional in AD (59,60). The DMN, which is preferentially disrupted in AD, is associated not only with various cognitive functions and episodic memory but also with amyloid deposits (29,30). Our study shows that these predominantly DMN-related alterations seem to reflect a subgroup of AD individuals (around 31%) while the other

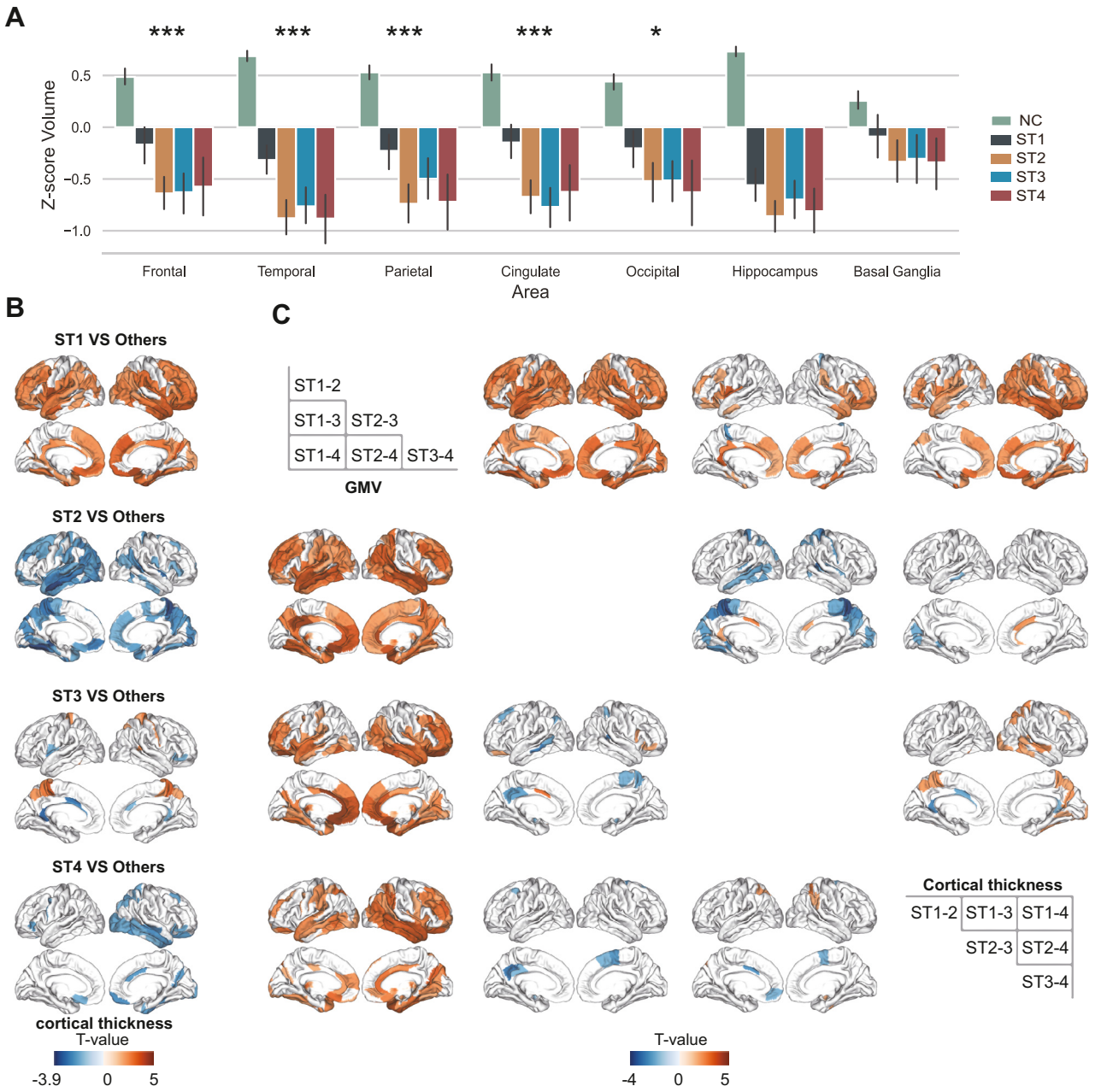

Figure 4. Analysis of the structural characteristics between the subtypes in Alzheimer's disease. **(A)** The bar figure shows the regional mean *z* score volumes of the subtypes and the normal control subjects (NCs). All the brain regions showed significantly decreased gray matter volume (GMV) compared with those of NCs ($p < .001$); *represents the *p* values of analysis of variance between subtypes. **(B)** One-to-others cortical thickness comparisons. The difference in the cortical thickness was obtained by comparing one subtype to the other subtypes ("Others" in the Figure) to show the subtype-specific anatomical characteristics. **(C)** The two-paired comparisons in GMV are shown in the left lower area, and the cortical thickness results are shown in the right upper area. *$p < .05$, ***$p < .001$. ST, subtype.

subgroups show different types of alterations. The ACC, which showed degeneration in the early stages of AD (61,62), accounts for the decline in diverse functional alterations from emotional processing and cognitive control regulation (subtype 3). Subtype 4 showed specific alterations associated with the basal ganglia (63), which are vitally important in normal brain functioning, including motor, cognition, and emotional processing (64). More importantly, several studies consistently found that functional connectivity within the frontal lobe is increasingly altered with the advancement of AD and aging (32,65–69). Although this increased alteration was hypothesized to be a complementary mechanism (70–72), the

underlying mechanism of this phenomenon is unclear. Our results showed a negative correlation between prefrontal connectivity and cognition, indicating that elevated prefrontal activity may accompany severe functional disruption.

The subtypes identified by functional connectivity also reflected considerable neurobiological and clinical heterogeneity. Individuals with subtype 1 had diffuse and mild functional connectivity disruption, structural atrophy, and overall cognitive decline, indicating that this subtype had the mildest pathological changes and was similar to what has previously been termed the mild atrophic subtype (18–20). Subtype 2 had the most widespread structural thinning and the worst cognitive ability, and therefore it is similar to the typical subtype of AD, which is based on neurofibrillary tangles and structural subtypes (13,18–20). Subtype 3 had more severe atrophy in the ACC and ventral cingulate cortex but had higher paracentral lobule and precuneus volumes, higher word learning ability (Auditory Verbal Learning Test), the slowest decrease in MMSE scores, and a relatively high volume in the hippocampus. Subtype 3 had some features of the posterior subtype (subtype 3) in the tau-PET study (26), which was accounted for as the posterior cortical atrophy (73). This atypical functional impairment partially explained the damage to the cognitive profiles in posterior cortical atrophy, e.g., low visuospatial ability and high word learning ability (74–76). Subtype 4 had serious dysfunction in the connections between the bilateral caudate and the occipital and parietal lobes and the cerebellum, right-lateralized visual cortex volume loss, lower word learning ability (Auditory Verbal Learning Test), and lower ADNI-VS levels, corresponding to some features of the corticobasal syndrome (77,78). Our results showed that heterogeneity in brain networks manifests along a continuum in AD, and atypical clinical variants may represent the extremes in the AD continuum (21,26). Finally, although our subtypes did not show a one-to-one correspondence with previous subtyping studies, it is interesting that our functional subtypes also had a 2-dimensional framework (severity vs. typicality) of AD subtyping (4): subtype 1 and subtype 2 seemed consistent with the severity axis, whereas subtype 3 and subtype 4 seemed consistent with the typicality axis.

Finding subtype divisions in MCI provided additional information about predementia stage conditions (79–81). In both datasets, nearly 45% of the MCI participants were classified into the mildest impairment subtype based on AD parameters. This finding was plausible because people with MCI generally have mild functional alterations and cognitive impairments (20). Moreover, it also shows that our model did not merely capture information about the severity of AD. Importantly, the MCI participants showed similar patterns of differential functional connectivity and cognition to those found in patients with AD, indicating that abnormal network heterogeneity exists in the early stage of AD. No apparent cognitive differentiation was found, suggesting that there is an underlying functional heterogeneity despite the macroscopic-level homogeneity in the MCI stage.

It should be emphasized that our findings were highly reliable and reproducible. The abnormal network used in the present study, which was derived from a reliable multicentric mega-analysis study (40), overlapped with the DMN, salience network, executive network, and several subcortical areas. The RFNs of the subtypes were derived from the AFN by investigating the coherent patterns of functional connectivity across subjects using NMF. In total, 4 highly consistent RFNs and 3 highly correlated patterns of functional alteration were found in 2 completely independent datasets, which suggests that these patterns reflect biological differences between AD subgroups. It should also be noted that the uncorrelated impairments of subtype 1 between the 2 datasets might be attributed to the slight and nonspecific impairments (Figure S7). Moreover, RFNs and subtypes were stable when applied to different parcellation schema, with or without head motion control and with or without ComBat harmonization (Figures S4–S6).

This study had several limitations. First, confounding effects from the disease severity cannot be prevented completely in the present method, and the confounding information needs to be validated with longitudinal data in the future. Second, the individuals in the MCADI lacked pathological data. Thus, we only selected amyloid-β-positive individuals in the ADNI to reduce the effect of this issue, and our highly reproducible results may indicate that non-AD factors had little impact. Third, the sample size of the longitudinal data was still relatively small. Future studies with a large sample size that will include more neurobiological data (i.e., imaging data of amyloid-β and/or tau) are also needed to verify the relationship between the functional network divergence and AD-specific disease processes. Fourth, ComBat was validated on fMRI data but not applied generally, indicating that we cannot fully predict the changes in functional connectivity during harmonization (47). In addition, whether variations among scanners were controlled is unknown; this variation might also contribute to the uncorrelated alteration patterns of subtype 1 between the 2 datasets (Figure S7), which should be validated using more datasets. Finally, the relationship between functional subtypes and other modal subtypes (i.e., neurofibrillary tangles and structural- and PET-derived subtypes) needs to be investigated to uncover the heterogeneity of AD systematically.

Collectively, the present study comprehensively characterized AD-associated functional brain subtypes using two of the world's largest AD resting-state fMRI biobanks. Specific functional connectivity, cognitive function, and brain structure characteristics were found in these functional subtypes in both AD and MCI individuals. These comprehensive findings highlight the potential for identifying reproducible and generalizable functional brain subtypes that can contribute to identifying prognostic markers, provide important insight for reconciling categorical and dimensional perspectives, and thus advance the progress toward future precision clinical trials that will be able to target specific subtypes of AD.

ACKNOWLEDGMENTS AND DISCLOSURES

This work was partially supported by the Fundamental Research Funds for the Central Universities (Grant No. 2021XD-A03-1 [to YL]), the Beijing Natural Science Funds for Distinguished Young Scholars (Grant No. JQ20036 [to YL]), the National Natural Science Foundation of China (Grant Nos. 81871438 [to YL], 82172018 [to YL], and 81901101 [to PW]), and the Special Fund for Military Health committee (Grant No. 21BJZ21 [to HYao]). Data collection and sharing for this project were funded by the National Natural Science Foundation of China (Grant Nos. 61633018 [to YH], 81571062 [to YL], 81400890 [to DW], and 81471120 [to XZ]).

Data collection and sharing for this project were funded by the ADNI (National Institutes of Health Grant No. U01 AG024904) and DOD ADNI

(Department of Defense Award Number W81XWH-12-2-0012). ADNI is funded by the National Institute on Aging, the National Institute of Biomedical Imaging and Bioengineering, and through generous contributions from the following: AbbVie, Alzheimer's Association; Alzheimer's Drug Discovery Foundation; Araclon Biotech; BioClinica, Inc.; Biogen; Bristol-Myers Squibb Company; CereSpir, Inc.; Cogstate; Eisai Co., Inc.; Elan Pharmaceuticals, Inc.; Eli Lilly and Company; EUROIMMUN; F. Hoffmann-La Roche Ltd and its affiliated company Genentech, Inc.; Fujirebio; GE Healthcare; IXICO Ltd.; Janssen Alzheimer Immunotherapy Research & Development, LLC.; Johnson & Johnson Pharmaceutical Research & Development, LLC.; Lumosity; Lundbeck; Merck & Co., Inc.; Meso Scale Diagnostics, LLC.; NeuroRx; Neurotrack Technologies, Inc; Novartis Pharmaceuticals Corporation; Pfizer Inc.; Piramal Imaging; Servier; Takeda Pharmaceutical Company; and Transition Therapeutics. The Canadian Institutes of Health Research provides funds to support ADNI clinical sites in Canada. Private sector contributions are facilitated by the Foundation for the National Institutes of Health (http://www.fnih.org). The grantee organization is the Northern California Institute for Research and Education, and the study is coordinated by the Alzheimer's Therapeutic Research Institute at the University of Southern California. ADNI data are disseminated by the Laboratory for Neuro Imaging at the University of Southern California.

We thank Drs. Rhoda E. and Edmund F. Perozzi for their very extensive English language and editing assistance.

Data used in preparation of this article were obtained from the Alzheimer's Disease Neuroimaging Initiative (ADNI) database (http://adni.loni.usc.edu). As such, the investigators within the ADNI contributed to the design and implementation of ADNI and/or provided data but did not participate in the analysis or writing of this report. A complete listing of the ADNI investigators can be found at: http://adni.loni.usc.edu/wp-content/uploads/how_to_apply/ADNI_Acknowledgement_List.pdf

The authors report no biomedical financial interests or potential conflicts of interest.

ARTICLE INFORMATION

From the Brainnetome Center & National Laboratory of Pattern Recognition (PC, YQ, XK, KD, LF, TJ, YL), Institute of Automation, Chinese Academy of Sciences; the School of Artificial Intelligence (PC, YQ, XK, KD, TJ, YL), University of Chinese Academy of Sciences; Department of Radiology (HYao) and Department of Neurology (XZ, BZ), the Second Medical Centre, National Clinical Research Centre for Geriatric Diseases, Chinese PLA General Hospital; Department of Radiology (HYang, JL) and Department of Neurology (YH), Xuanwu Hospital of Capital Medical University; Beijing Advanced Innovation Center for Biomedical Engineering (KZ), School of Biological Science & Medical Engineering, Beihang University; Beijing Institute of Geriatrics (YH); National Clinical Research Center for Geriatric Disorders (YH); State Key Laboratory of Cognition Neuroscience & Learning (BL), Beijing Normal University; School of Artificial Intelligence (YL), Beijing University of Posts and Telecommunications, Beijing; Department of Neurology (PW, YZ) and Department of Radiology (TH), Tianjin Huanhu Hospital, Tianjin University; Department of Radiology (CY), Tianjin Medical University General Hospital, Tianjin; Department of Radiology (DW) and Department of Neurology (CS), Qilu Hospital of Shandong University, Ji'nan; Branch of Chinese PLA General Hospital (ZZ), Sanya, China; and the Alzheimer Center Amsterdam (BMT), Department of Neurology, Amsterdam Neuroscience, Vrije Universiteit Amsterdam, Amsterdam UMC - Location VUmc, The Netherlands.

PC and HYao contributed equally to this work.

Address correspondence to Bo Zhou, M.D., at zhoubo@301hospital.com.cn, or Yong Liu, Ph.D., at yongliu@bupt.edu.cn.

Received Jan 13, 2022; revised May 19, 2022; accepted Jun 13, 2022.

Supplementary material cited in this article is available online at https://doi.org/10.1016/j.biopsych.2022.06.019.

REFERENCES

1. Lam B, Masellis M, Freedman M, Stuss DT, Black SE (2013): Clinical, imaging, and pathological heterogeneity of the Alzheimer's disease syndrome. Alzheimers Res Ther 5:1.
2. Roe CM, Fagan AM, Williams MM, Ghoshal N, Aeschleman M, Grant EA, *et al.* (2011): Improving CSF biomarker accuracy in predicting prevalent and incident Alzheimer disease. Neurology 76:501–510.
3. Graff-Radford J, Yong KXX, Apostolova LG, Bouwman FH, Carrillo M, Dickerson BC, *et al.* (2021): New insights into atypical Alzheimer's disease in the era of biomarkers. Lancet Neurol 20:222–234.
4. Ferreira D, Nordberg A, Westman E (2020): Biological subtypes of Alzheimer disease: A systematic review and meta-analysis. Neurology 94:436–448.
5. McKhann GM, Knopman DS, Chertkow H, Hyman BT, Jack CR Jr, Kawas CH, *et al.* (2011): The diagnosis of dementia due to Alzheimer's disease: Recommendations from the National Institute on Aging-Alzheimer's Association workgroups on diagnostic guidelines for Alzheimer's disease. Alzheimers Dement 7:263–269.
6. Jack CR Jr, Albert MS, Knopman DS, McKhann GM, Sperling RA, Carrillo MC, *et al.* (2011): Introduction to the recommendations from the National Institute on Aging-Alzheimer's Association workgroups on diagnostic guidelines for Alzheimer's disease. Alzheimers Dement 7:257–262.
7. Crist AM, Hinkle KM, Wang X, Moloney CM, Matchett BJ, Labuzan SA, *et al.* (2021): Transcriptomic analysis to identify genes associated with selective hippocampal vulnerability in Alzheimer's disease. Nat Commun 12:2311.
8. Drummond E, Nayak S, Faustin A, Pires G, Hickman RA, Askenazi M, *et al.* (2017): Proteomic differences in amyloid plaques in rapidly progressive and sporadic Alzheimer's disease. Acta Neuropathol 133:933–954.
9. Risacher SL, Anderson WH, Charil A, Castelluccio PF, Shcherbinin S, Saykin AJ, *et al.* (2017): Alzheimer disease brain atrophy subtypes are associated with cognition and rate of decline. Neurology 89:2176–2186.
10. Ossenkoppele R, Lyoo CH, Sudre CH, van Westen D, Cho H, Ryu YH, *et al.* (2020): Distinct tau PET patterns in atrophy-defined subtypes of Alzheimer's disease. Alzheimers Dement 16:335–344.
11. Whitwell JL, Dickson DW, Murray ME, Weigand SD, Tosakulwong N, Senjem ML, *et al.* (2012): Neuroimaging correlates of pathologically defined subtypes of Alzheimer's disease: A case-control study. Lancet Neurol 11:868–877.
12. Jellinger KA (2012): Neuropathological subtypes of Alzheimer's disease. Acta Neuropathol 123:153–154.
13. Murray ME, Graff-Radford NR, Ross OA, Petersen RC, Duara R, Dickson DW (2011): Neuropathologically defined subtypes of Alzheimer's disease with distinct clinical characteristics: A retrospective study. Lancet Neurol 10:785–796.
14. Shima K, Matsunari I, Samuraki M, Chen WP, Yanase D, Noguchi-Shinohara M, *et al.* (2012): Posterior cingulate atrophy and metabolic decline in early stage Alzheimer's disease. Neurobiol Aging 33:2006–2017.
15. Oppedal K, Ferreira D, Cavallin L, Lemstra AW, Ten Kate M, Padovani A, *et al.* (2019): A signature pattern of cortical atrophy in dementia with Lewy bodies: A study on 333 patients from the European DLB Consortium. Alzheimers Dement 15:400–409.
16. Ferreira D, Shams S, Cavallin L, Viitanen M, Martola J, Granberg T, *et al.* (2018): The contribution of small vessel disease to subtypes of Alzheimer's disease: A study on cerebrospinal fluid and imaging biomarkers. Neurobiol Aging 70:18–29.
17. Noh Y, Jeon S, Lee JM, Seo SW, Kim GH, Cho H, *et al.* (2014): Anatomical heterogeneity of Alzheimer disease: Based on cortical thickness on MRIs. Neurology 83:1936–1944.
18. Dong A, Toledo JB, Honnorat N, Doshi J, Varol E, Sotiras A, *et al.* (2017): Heterogeneity of neuroanatomical patterns in prodromal Alzheimer's disease: Links to cognition, progression and biomarkers. Brain 140:735–747.
19. Poulakis K, Pereira JB, Mecocci P, Vellas B, Tsolaki M, Kłoszewska I, *et al.* (2018): Heterogeneous patterns of brain atrophy in Alzheimer's disease. Neurobiol Aging 65:98–108.
20. Ten Kate M, Dicks E, Visser PJ, van der Flier WM, Teunissen CE, Barkhof F, *et al.* (2018): Atrophy subtypes in prodromal Alzheimer's

disease are associated with cognitive decline. Brain 141:3443–3456.
21. Sun N, Mormino EC, Chen J, Sabuncu MR, Yeo BTT, Alzheimer's Disease Neuroimaging initiative (2019): Multi-modal latent factor exploration of atrophy, cognitive and tau heterogeneity in Alzheimer's disease. Neuroimage 201:116043.
22. Sui X, Rajapakse JC, Alzheimer's Disease Neuroimaging Initiative (2018): Profiling heterogeneity of Alzheimer's disease using white-matter impairment factors. Neuroimage Clin 20:1222–1232.
23. Levin F, Ferreira D, Lange C, Dyrba M, Westman E, Buchert R, *et al.* (2021): Data-driven FDG-PET subtypes of Alzheimer's disease-related neurodegeneration. Alzheimers Res Ther 13:49.
24. Lowe VJ, Wiste HJ, Senjem ML, Weigand SD, Therneau TM, Boeve BF, *et al.* (2018): Widespread brain tau and its association with ageing, Braak stage and Alzheimer's dementia. Brain 141:271–287.
25. Whitwell JL, Graff-Radford J, Tosakulwong N, Weigand SD, Machulda M, Senjem ML, *et al.* (2018): [^{18} F]AV-1451 clustering of entorhinal and cortical uptake in Alzheimer's disease. Ann Neurol 83:248–257.
26. Vogel JW, Young AL, Oxtoby NP, Smith R, Ossenkoppele R, Strandberg OT, *et al.* (2021): Four distinct trajectories of tau deposition identified in Alzheimer's disease. Nat Med 27:871–881.
27. Collij LE, Salvadó G, Wottschel V, Mastenbroek SE, Schoenmakers P, Heeman F, *et al.* (2022): Spatial-temporal patterns of β-amyloid accumulation: A subtype and stage inference model analysis. Neurology 98:e1692–e1703.
28. Dai Z, He Y (2014): Disrupted structural and functional brain connectomes in mild cognitive impairment and Alzheimer's disease. Neurosci Bull 30:217–232.
29. Dennis EL, Thompson PM (2014): Functional brain connectivity using fMRI in aging and Alzheimer's disease. Neuropsychol Rev 24:49–62.
30. Eyler LT, Elman JA, Hatton SN, Gough S, Mischel AK, Hagler DJ, *et al.* (2019): Resting state abnormalities of the default mode network in mild cognitive impairment: A systematic review and meta-analysis. J Alzheimers Dis 70:107–120.
31. Wang J, Zuo X, Dai Z, Xia M, Zhao Z, Zhao X, *et al.* (2013): Disrupted functional brain connectome in individuals at risk for Alzheimer's disease. Biol Psychiatry 73:472–481.
32. Liu Y, Yu C, Zhang X, Liu J, Duan Y, Alexander-Bloch AF, *et al.* (2014): Impaired long distance functional connectivity and weighted network architecture in Alzheimer's disease. Cereb Cortex 24:1422–1435.
33. Zhou B, Yao H, Wang P, Zhang Z, Zhan Y, Ma J, *et al.* (2015): Aberrant functional connectivity architecture in Alzheimer's disease and mild cognitive impairment: A whole-brain, data-driven analysis. BioMed Res Int 2015:495375.
34. Hahn A, Strandberg TO, Stomrud E, Nilsson M, van Westen D, Palmqvist S, *et al.* (2019): Association between earliest amyloid uptake and functional connectivity in cognitively unimpaired elderly. Cereb Cortex 29:2173–2182.
35. Zhou J, Gennatas ED, Kramer JH, Miller BL, Seeley WW (2012): Predicting regional neurodegeneration from the healthy brain functional connectome. Neuron 73:1216–1227.
36. Jones DT, Graff-Radford J, Lowe VJ, Wiste HJ, Gunter JL, Senjem ML, *et al.* (2017): Tau, amyloid, and cascading network failure across the Alzheimer's disease spectrum. Cortex 97:143–159.
37. Guzmán-Vélez E, Diez I, Schoemaker D, Pardilla-Delgado E, Vila-Castelar C, Fox-Fuller JT, *et al.* (2022): Amyloid-β and tau pathologies relate to distinctive brain dysconnectomics in preclinical autosomal-dominant Alzheimer's disease. Proc Natl Acad Sci U S A 119: e2113641119.
38. Seeley WW, Crawford RK, Zhou J, Miller BL, Greicius MD (2009): Neurodegenerative diseases target large-scale human brain networks. Neuron 62:42–52.
39. Rauchmann BS, Ersoezlue E, Stoecklein S, Keeser D, Brosseron F, Buerger K, *et al.* (2021): Resting-state network alterations differ between Alzheimer's disease atrophy subtypes. Cereb Cortex 31:4901–4915.
40. Jin D, Wang P, Zalesky A, Liu B, Song C, Wang D, *et al.* (2020): GrabAD: Generalizability and reproducibility of altered brain activity and diagnostic classification in Alzheimer's disease. Hum Brain Mapp 41:3379–3391.
41. Qu Y, Wang P, Liu B, Song C, Wang D, Yang H, *et al.* (2021): AI4AD: Artificial intelligence analysis for Alzheimer's disease classification based on a multisite DTI database. Brain Disord 1:100005.
42. Li JC, Jin D, Li A, Liu B, Song C, Wang P, *et al.* (2019): ASAF: Altered spontaneous activity fingerprinting in Alzheimer's disease based on multisite fMRI. Sci Bull 64:998–1010.
43. Fan L, Li H, Zhuo J, Zhang Y, Wang J, Chen L, *et al.* (2016): The human Brainnetome atlas: A new brain atlas based on connectional architecture. Cereb Cortex 26:3508–3526.
44. Johnson WE, Li C, Rabinovic A (2007): Adjusting batch effects in microarray expression data using empirical Bayes methods. Biostatistics 8:118–127.
45. Fortin JP, Cullen N, Sheline YI, Taylor WD, Aselcioglu I, Cook PA, *et al.* (2018): Harmonization of cortical thickness measurements across scanners and sites. Neuroimage 167:104–120.
46. Xu K, Liu Y, Zhan Y, Ren J, Jiang T (2018): BRANT: A versatile and extendable resting-state fMRI toolkit. Front Neuroinform 12:52.
47. Yu M, Linn KA, Cook PA, Phillips ML, McInnis M, Fava M, *et al.* (2018): Statistical harmonization corrects site effects in functional connectivity measurements from multi-site fMRI data. Hum Brain Mapp 39:4213–4227.
48. Lee DD, Seung HS (1999): Learning the parts of objects by non-negative matrix factorization. Nature 401:788–791.
49. Brunet JP, Tamayo P, Golub TR, Mesirov JP (2004): Metagenes and molecular pattern discovery using matrix factorization. Proc Natl Acad Sci U S A 101:4164–4169.
50. Gaujoux R, Seoighe C (2010): A flexible R package for nonnegative matrix factorization. BMC Bioinformatics 11:367.
51. Mohanty R, Mårtensson G, Poulakis K, Muehlboeck JS, Rodriguez-Vieitez E, Chiotis K, *et al.* (2020): Comparison of subtyping methods for neuroimaging studies in Alzheimer's disease: A call for harmonization. Brain Commun 2:fcaa192.
52. Habes M, Grothe MJ, Tunc B, McMillan C, Wolk DA, Davatzikos C (2020): Disentangling heterogeneity in Alzheimer's disease and related dementias using data-driven methods. Biol Psychiatry 88:70–82.
53. Schwarz CG, Gunter JL, Wiste HJ, Przybelski SA, Weigand SD, Ward CP, *et al.* (2016): A large-scale comparison of cortical thickness and volume methods for measuring Alzheimer's disease severity. NeuroImage Clin 11:802–812.
54. Satterthwaite TD, Wolf DH, Loughead J, Ruparel K, Elliott MA, Hakonarson H, *et al.* (2012): Impact of in-scanner head motion on multiple measures of functional connectivity: Relevance for studies of neurodevelopment in youth. Neuroimage 60:623–632.
55. Zhang B, Lin L, Wu S, Al-Masqari ZHMA (2021): Multiple subtypes of Alzheimer's disease base on brain atrophy pattern. Brain Sci 11:278.
56. Tijms BM, Gobom J, Reus L, Jansen I, Hong S, Dobricic V, *et al.* (2020): Pathophysiological subtypes of Alzheimer's disease based on cerebrospinal fluid proteomics. Brain 143:3776–3792.
57. Machado A, Ferreira D, Grothe MJ, Eyjolfsdottir H, Almqvist PM, Cavallin L, *et al.* (2020): The cholinergic system in subtypes of Alzheimer's disease: An in vivo longitudinal MRI study. Alzheimers Res Ther 12:51.
58. Ezzati A, Zammit AR, Habeck C, Hall CB, Lipton RB, Alzheimer's Disease Neuroimaging initiative (2020): Detecting biological heterogeneity patterns in ADNI amnestic mild cognitive impairment based on volumetric MRI. Brain Imaging Behav 14:1792–1804.
59. Tetreault AM, Phan T, Orlando D, Lyu I, Kang H, Landman B, *et al.* (2020): Network localization of clinical, cognitive, and neuropsychiatric symptoms in Alzheimer's disease. Brain 143:1249–1260.
60. Dai Z, Lin Q, Li T, Wang X, Yuan H, Yu X, *et al.* (2019): Disrupted structural and functional brain networks in Alzheimer's disease. Neurobiol Aging 75:71–82.
61. Jones BF, Barnes J, Uylings HBM, Fox NC, Frost C, Witter MP, Scheltens P (2006): Differential regional atrophy of the cingulate gyrus in Alzheimer disease: A volumetric MRI study. Cereb Cortex 16:1701–1708.
62. Amanzio M, Torta DME, Sacco K, Cauda F, D'Agata F, Duca S, *et al.* (2011): Unawareness of deficits in Alzheimer's disease: Role of the cingulate cortex. Brain 134:1061–1076.

63. Bostan AC, Strick PL (2018): The basal ganglia and the cerebellum: Nodes in an integrated network. Nat Rev Neurosci 19:338–350.
64. Cho H, Kim JH, Kim C, Ye BS, Kim HJ, Yoon CW, *et al.* (2014): Shape changes of the basal ganglia and thalamus in Alzheimer's disease: A three-year longitudinal study. J Alzheimers Dis 40:285–295.
65. Wang K, Liang M, Wang L, Tian L, Zhang X, Li K, Jiang T (2007): Altered functional connectivity in early Alzheimer's disease: A resting-state fMRI study. Hum Brain Mapp 28:967–978.
66. Sanz-Arigita EJ, Schoonheim MM, Damoiseaux JS, Rombouts SA, Maris E, Barkhof F, *et al.* (2010): Loss of 'small-world' networks in Alzheimer's disease: Graph analysis of FMRI resting-state functional connectivity. PLoS One 5:e13788.
67. Agosta F, Pievani M, Geroldi C, Copetti M, Frisoni GB, Filippi M (2012): Resting state fMRI in Alzheimer's disease: Beyond the default mode network. Neurobiol Aging 33:1564–1578.
68. Ewers M, Luan Y, Frontzkowski L, Neitzel J, Rubinski A, Dichgans M, *et al.* (2021): Segregation of functional networks is associated with cognitive resilience in Alzheimer's disease. Brain 144:2176–2185.
69. Chan MY, Park DC, Savalia NK, Petersen SE, Wig GS (2014): Decreased segregation of brain systems across the healthy adult lifespan. Proc Natl Acad Sci U S A 111:E4997–E5006.
70. Bai F, Watson DR, Yu H, Shi Y, Yuan Y, Zhang Z (2009): Abnormal resting-state functional connectivity of posterior cingulate cortex in amnestic type mild cognitive impairment. Brain Res 1302: 167–174.
71. Qi Z, Wu X, Wang Z, Zhang N, Dong H, Yao L, Li K (2010): Impairment and compensation coexist in amnestic MCI default mode network. Neuroimage 50:48–55.
72. Arenaza-Urquijo EM, Landeau B, La Joie R, Mevel K, Mézenge F, Perrotin A, *et al.* (2013): Relationships between years of education and gray matter volume, metabolism and functional connectivity in healthy elders. Neuroimage 83:450–457.
73. Mendez MF, Ghajarania M, Perryman KM (2002): Posterior cortical atrophy: Clinical characteristics and differences compared to Alzheimer's disease. Dement Geriatr Cogn Disord 14:33–40.
74. Novais F, Starkstein S (2015): Phenomenology of depression in Alzheimer's disease. J Alzheimers Dis 47:845–855.
75. Elsworthy RJ, Aldred S (2019): Depression in Alzheimer's disease: An alternative role for selective serotonin reuptake inhibitors? J Alzheimers Dis 69:651–661.
76. Aalten P, Verhey FRJ, Boziki M, Bullock R, Byrne EJ, Camus V, *et al.* (2007): Neuropsychiatric syndromes in dementia. Results from the European Alzheimer disease Consortium: Part I. Dement Geriatr Cogn Disord 24:457–463.
77. Di Stasio F, Suppa A, Marsili L, Upadhyay N, Asci F, Bologna M, *et al.* (2019): Corticobasal syndrome: Neuroimaging and neurophysiological advances. Eur J Neurol 26:701–e52.
78. Ossenkoppele R, Schonhaut DR, Schöll M, Lockhart SN, Ayakta N, Baker SL, *et al.* (2016): Tau PET patterns mirror clinical and neuroanatomical variability in Alzheimer's disease. Brain 139:1551–1567.
79. Kim HJ, Park JY, Seo SW, Jung YH, Kim Y, Jang H, *et al.* (2019): Cortical atrophy pattern-based subtyping predicts prognosis of amnestic MCI: An individual-level analysis. Neurobiol Aging 74:38–45.
80. Jung NY, Seo SW, Yoo H, Yang JJ, Park S, Kim YJ, *et al.* (2016): Classifying anatomical subtypes of subjective memory impairment. Neurobiol Aging 48:53–60.
81. Zhao K, Zheng Q, Dyrba M, Rittman T, Li A, Che T, *et al.* (2022): Regional radiomics similarity networks reveal distinct subtypes and abnormality patterns in mild cognitive impairment. Adv Sci (Weinh) 9: e2104538.